Seasonal Variability of Mercury's Sodium Exosphere Deduced from MESSENGER Data and Numerical Simulation

Yudai Suzuki[1], Kazuo Yoshioka[2], Go Murakami[3], and Ichiro Yoshikawa[1]

[1]University of Tokyo
[2]The University of Tokyo
[3]Japan Aerospace Exploration Agency

November 24, 2022

Abstract

Mercury is valuable to us because we can see the interaction between the planet and its space environment. This research aims to clarify how Mercury's neutral Na exosphere was produced. Data from MESSENGER/MASCS and model calculations that examine possible generation, transportation and dissipation processes will be compared. First, seasonal variability of the amount of Na exosphere is analyzed for each local time (LT) using MASCS data. Previous research has shown that the amount of Na above LT12 reaches its maximum at aphelion, and it is found that this maximum is recorded only at LT12. Following this result, we construct 3-D Na exosphere model to understand the key seasonal variability processes occurring around LT12. The numerical calculation produced results that are consistent with the MASCS observations regarding the vertical profile and the seasonal variability at LT06 and LT18. However, the peak that occurs around aphelion at LT12 could not be reproduced. Yet the model produced results suggesting that less than 10 kg particles of comet stream dust per Mercury year could be the local and short-term source of Na.

Seasonal Variability of Mercury's Sodium Exosphere Deduced from MESSENGER Data and Numerical Simulation

Y. Suzuki[1], K. Yoshioka[1], G. Murakami[2], I. Yoshikawa[1]

[1] The University of Tokyo, [2] ISAS/JAXA

Corresponding author: Yudai Suzuki (yudai-suzuki127@g.ecc.u-tokyo.ac.jp)

Key Points:

- The seasonal variability of Mercury's Na exosphere is investigated using observations by MESSENGER/MASCS and a 3-D Monte Carlo model.
- Theoretical model that considers only four processes: TD, PSD, SWS, and MIV, does not reproduce the peak around aphelion at LT12.
- The putative presence of comet dust streams could resolve this inconsistency.

Abstract

Mercury is valuable to us because we can see the interaction between the planet and its space environment. This research aims to clarify how Mercury's neutral Na exosphere was produced. Data from MESSENGER/MASCS and model calculations that examine possible generation, transportation and dissipation processes will be compared. First, seasonal variability of the amount of Na exosphere is analyzed for each local time (LT) using MASCS data. Previous research has shown that the amount of Na above LT12 reaches its maximum at aphelion, and it is found that this maximum is recorded only at LT12. Following this result, we construct 3-D Na exosphere model to understand the key seasonal variability processes occurring around LT12. The numerical calculation produced results that are consistent with the MASCS observations regarding the vertical profile and the seasonal variability at LT06 and LT18. However, the peak that occurs around aphelion at LT12 could not be reproduced. Yet the model produced results suggesting that less than 10^8 kg particles of comet stream dust per Mercury year could be the local and short-term source of Na.

Plain Language Summary

The seasonal variability of Mercury's Na exosphere is investigated using optical observations by MESSENGER spacecraft and a 3-D Monte Carlo model. Analysis of observations shows that the amount of Na exosphere increases around aphelion at noon. Theoretical model that considers physical processes of outgassing and particle transportation does not reproduce this local and short-term increase. The putative presence of comet dust streams could resolve this inconsistency.

1 Introduction

The components of Mercury's exosphere except H and He are released from the surface by several desorption mechanisms under the influence of the surrounding space environment. These mechanisms are listed as Thermal Desorption (TD), Photo Stimulated Desorption (PSD), Charged Particle Sputtering (CPS) and Micrometeoroid Impact Vaporization (MIV). Because of the great eccentricity and inclination of its orbit, Mercury's exospheric volume varies significantly following its orbital phases (True Anomaly Angle: TAA). Consequent to the extremely long mean free path in the exosphere, the spatial and energy distributions of desorbed atoms are directly observable in the exospheric structure. Based on these characteristics, Mercury is an important source of data where the effects of the space environment on it can be observed directly.

Building an exospheric model is a powerful tool, especially for Mercury, which is difficult to observe frequently. In Leblanc and Johnson (2003, 2010), the seasonal variability of the global ejection rate from each desorption mechanism was evaluated. This was done by reproducing the ground observation results, and they determined that the dominant ejection mechanism differs depending on TAA. Mura et al. (2009) suggested that solar wind photon precipitation could be freeing sodium atoms from their crystalline structures (chemical sputtering) and making them more easily ejected by TD and PSD, by comparing the Schleicher et al. (2004) observations which show a dawn-dusk asymmetry and the maximum near the polar regions with north prevalence. Burger et al. (2010) and Wang and Ip (2011) established models and compared them with the data obtained by MESSENGER during its flybys. The former paper demonstrates that the PSD desorption rate is limited by the diffusion rate of Na from the interior of the regolith to the surface and that the precipitation of ions enhances diffusion rate at high latitudes. The latter suggests that the binding energy is not strongly surface temperature-dependent and should be close to zero. These models significantly improved our understanding of the dynamics of the Na exosphere of Mercury. However, the parameters used in these studies differ among models. Additionally, many models are based on ground observations or MESSENGER's flyby-data, but few model studies have focused on the fine spatial structure found by MESSENGER's orbiting observations.

The only spacecraft that has orbited Mercury is NASA's MESSENGER from 2004 to 2015. The Mercury Atmospheric and Surface Composition Spectrometer (MASCS) onboard MESSENGER mainly observed the radiance of Na, Ca and Mg in the exosphere during the atmospheric mode (McClintock and Lankton, 2007). The UVVS channel of MASCS has provided almost daily observations of the exosphere. Its data reveal that Na in the exosphere below an altitude of 1,000 km is ejected mainly by PSD, although above 1,000 km the main Na ejection process is still unknown (Cassidy et al., 2015). The seasonal variability of the density of the Na exosphere was also estimated in the same study. As a result, the amount of Na above Local Time (LT) 12 was surprisingly high, even around aphelion. This peak was not anticipated by ground observations or qualitative predictions because Mercury's dayside cannot be observed from Earth. In this paper, we discuss this surprising peak at aphelion using both MASCS data and numerical calculations using a Monte Carlo simulation.

2 Na distribution deduced from the MASCS data

We estimated the seasonal variability of Na emissions through analysis of the limb-scan data obtained by MASCS. We extract the data for which z-component of unit boresight vector is larger than 0.9, that is, the data of observations from south to true north (**Fig. 1**). **Fig. 2(a)** shows the seasonal variability of the Na exosphere at an altitude of 300 km above LT06, LT12 and LT18. Observables are equivalent to the line-of-sight integral of the radiation due to resonant scattering of Na, but we regard these integrated values as the radiation at the corresponding tangential altitude because it is believed that the amount of exosphere exponentially decreases as altitude increases (Chamberlain, 1963). The Na emission has its maximum at aphelion above LT12 as mentioned by Cassidy et al. (2015); however, it has a minimum above LT06 and LT18 also at aphelion. The observed radiance is the product of g-factor and column density. Then, by dividing the radiance by the g-factor, we obtain the seasonal variability of the Na column density, as shown in **Fig. 2(b)**. Note that seasonal variations in radiance does not always reflect the variability of column density since g-factor also varies seasonally. For example, the peak around TAA 40° at LT12 in **Fig. 2(a)** is not seen in **Fig. 2(b)**, which means this peak in radiance is the "apparent" one. It can be seen that the amount of Na has its maximum above LT12 and has a minimum above LT06 and LT18 around the aphelion. Though the trends of LT06 and LT18 are consistent with ground observations and qualitative prediction, which of LT12 is far from any

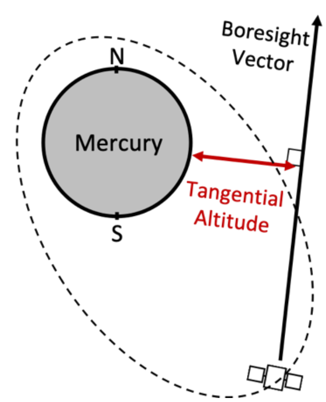

Fig. 1. Geometry of MESSENGER
MESSENGER orbits Mercury in a long north-south orbit with high eccentricity. The shortest distance between the boresight vector and the surface of Mercury is called tangential altitude.

former results of ground observations as also mentioned by Cassidy et al. (2015). Three possible reasons were suggested for this maximum at aphelion above LT12 by Cassidy et al. (2015, 2016): (1) the supply of surface Na-un-depleted from the nightside to the dayside by rotation, (2) the expansion of the exosphere of the dayside thanks to the weakening of solar radiation pressure, (3) the accumulation of Na on the “cold-pole longitude.” Since the maximum of LT12 would be caused by a combination of multiple factors, theoretical model that considers Na desorption and transport processes is required to verify hypotheses and identify the cause of seasonal variability of Na exosphere.

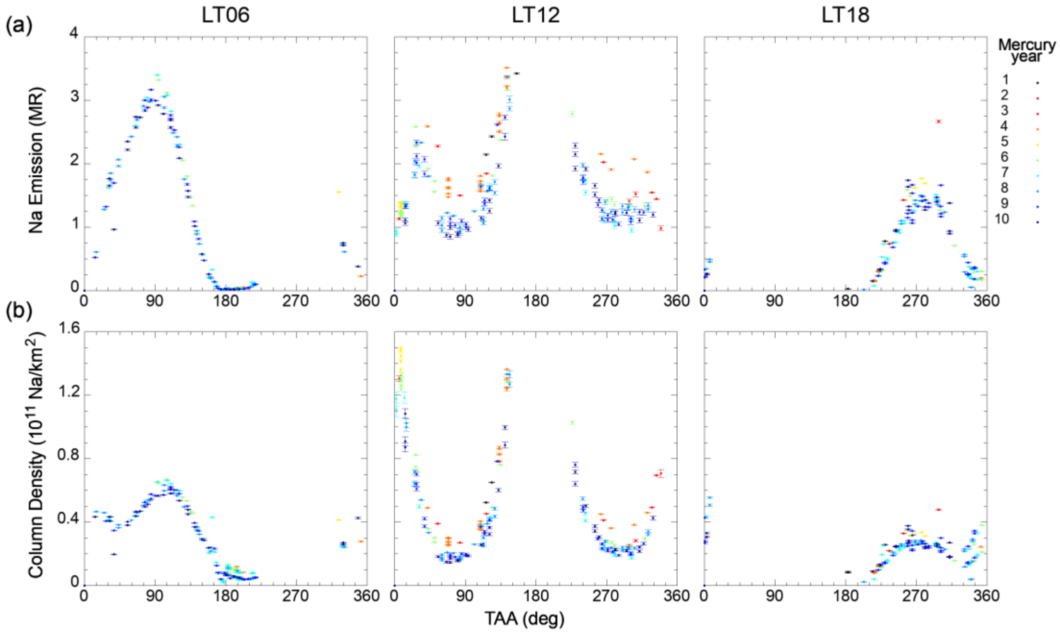

Fig. 2. The seasonal variability of Na exosphere deduced from MASCS data at various LTs (a) is illustrated by the radiance and (b) is illustrated by Na column density. Each symbol color represents Mercury year after orbit insertion of MESSENGER.

3 Settings of numerical calculation

To understand the key process dominating the seasonal variability of Na density, especially around LT12, we construct a 3-D Na exosphere model including desorption from the surface, transport due to gravity and solar radiation pressure, and loss due to re-impacting and photoionization. The initial surface density is set to be $1.5 \times 10^{23}\ \mathrm{Na/km^2}$ for the entire sphere with reference to Leblanc and Johnson (2003). The output is a value obtained by integrating the radiance in the line of sight when observed from the south.

3.1 Desorption processes

3.1.1 Thermal Desorption (TD)

Since Mercury revolves near the Sun and one Mercury day equals 176 Earth days, there is a large temperature gap between day and night. Infrared radiometry by Mariner 10 found the nightside temperature to be 100 K (Chase et al., 1976). Conversely, the model calculations show that the dayside reaches 700 K near the sub-solar point at perihelion (Vilas, 1988). The surface temperature can be estimated from the following equation with reference to Killen et al. (2004):

$$T_s = T_0 + T_1(\cos\phi\cos\lambda)^{\frac{1}{4}}\left(\frac{0.306\ \mathrm{au}}{r_0}\right)^2 \#(1)$$

ϕ, λ, r_0 are respectively, the latitude and longitude relative to the sub-solar point and the distance between the Sun and Mercury. T_0 and T_1 are 100 K and 600 K. As the surface temperature increases, atoms bound to the surface are released into the exosphere. The amount of released Na per surface unit per certain time (*dt*) is represented by following equation as a function of surface temperature:

$$R_{\mathrm{TD}} = \left[1 - \left\{1 - \exp\left(-\frac{U}{\mathrm{k_B}T_s}\right)\right\}^{\nu\,dt}\right]\sigma_{\mathrm{Na}}\#(2)$$

$\mathrm{k_B}$ is the Boltzmann constant and σ_{Na} is the surface density of Na. ν and U are the vibration frequency and binding energy of the Na atoms, respectively. Hunten and Sprague (2002) adopted $\nu = 10^{13}$Hz and $U = 1.4$eV, whereas Leblanc and Johnson (2010) assumes that $\nu = 10^9 - 10^{11}$Hz and defines U as a Gaussian distribution between 1.4 and 2.7 eV with a most probable value of 1.85 eV. In this model, we first set $\nu = 10^{13}$ Hz and $U = 1.85$ eV. $R_{\mathrm{TD}}/\sigma_{\mathrm{Na}}$ is shown in **Fig. 3** as a function of temperature. This figure implies that efficiency of TD greatly depends on temperature and the assumed parameters. The energy of released particles follows a Maxwellian distribution:

$$f(E,\theta) = \frac{2E}{(\mathrm{k_B}T)^2}\exp\left(-\frac{E}{\mathrm{k_B}T}\right)\cos\theta\ \#(3)$$

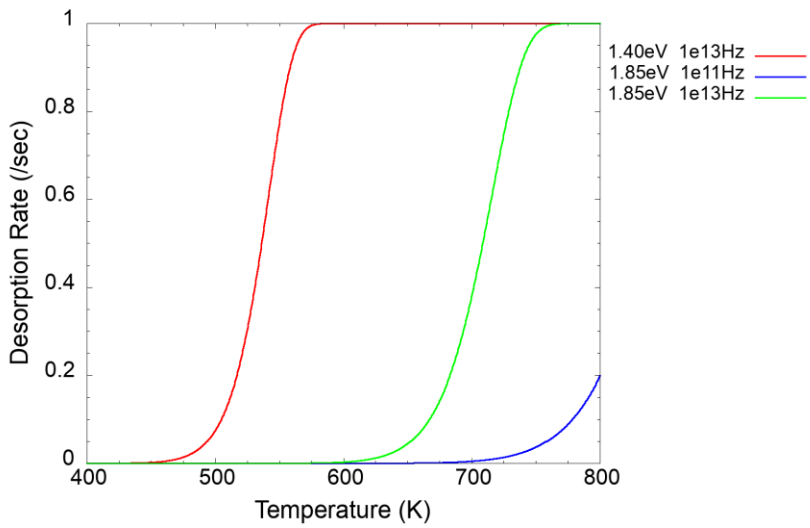

Fig. 3. Temperature dependence of efficiency of TD
Red line shows the settings of Hunten and Sprague (2002), blue one is that of Leblanc and Johnson (2010), and green one is that of this study.

E is the kinetic energy of particles and θ is the angle between normal vector to the surface and velocity vector. The surface temperature is shown as T. TD is expected to be enhanced around the perihelion and sub-solar point. The energy of released particles is too low to contribute directly to the structure of the exosphere. However, the migration of Na atoms through release and re-impact on the surface drastically varies the distribution of Na on the surface, with the result that TD controls the number of atoms released by other processes (e.g. Hunten and Sprague, 1997).

3.1.2 Photo Stimulated Desorption (PSD)

Mercury is always exposed to intense solar ultraviolet radiation. When electrons are excited by injected photons, they bond with Na^{+} ions on the surface, and neutral Na atoms are then ejected into the exosphere. The PSD ejection rate is estimated using the following equation:

$$R_{\mathrm{PSD}} = F_{\mathrm{UV}} Q_{\mathrm{PSD}} \cos Z\, c_{\mathrm{Na}} \#(4)$$

F_{UV}, Z and c_{Na} respectively represent the UV flux (inverse proportion to the square of the distance from the Sun), the solar zenith angle and the fraction of Na atoms in regolith. Although F_{UV} varies according to solar activity, we fix $F_{\mathrm{UV}} = 1.5 \times 10^{14}/(r_0/\mathrm{au})^2\ \mathrm{photon/cm^2/sec}$ at an average state. Q_{PSD} is the PSD cross-section, which is thought to depend on surface temperature (Yakshinskiy and Madey, 2004) and porosity (Cassidy and Johnson, 2005). Q_{PSD} is thought to be equal to $3 \times 10^{-20}\mathrm{cm^2}$ in Yakshinskiy and Madey (1999) from experiment, is set to $1.4 \times 10^{-21}\mathrm{cm^2}$ in Killen et al. (2004), and is assumed to be $2 \times 10^{-20}\mathrm{cm^2}$ in this study as a best fit parameter to the MASCS data. The energy of ejected particles is often fitted by a Maxwellian distribution, the temperature of which is 1,500 K based on an experiment by Yakshinskiy and Madey (1999). The rate of ejection by PSD increases around perihelion and sub-solar point as well as TD if the depletion of Na bound to the surface is not considered. From the estimation of the exospheric temperature based on observations by MASCS, Na atoms below 1,000 km altitude are thought to be ejected by PSD (Cassidy et al., 2015). Incident electrons can be an excitation source instead of UV (Electron Stimulated Desorption: ESD), but the flux of electrons is much smaller than that of UV. Therefore, ESD is ignored here.

3.1.3 Charged Particle Sputtering (CPS)

When ions impact the surface, atoms are emitted by momentum transfer. Ions are divided into two types: solar wind particles and those created by the ionization of neutral particles in the exosphere. The former case is called Solar Wind ion Sputtering (SWS) and the latter is called Magnetospheric Ion Sputtering (MIS). Since the flux of particles ionized in the exosphere is small (Delcourt et al., 2003), MIS is not examined in this study. The ejection rate by SWS was evaluated using the following equation:

$$R_{\mathrm{SWS}} = F_{\mathrm{SW}} Y_{\mathrm{SWS}} c_{\mathrm{Na}} \#(5)$$

F_{SW} is the flux of the impacted solar wind particles, which can be estimated by the product of solar wind velocity v_{SW} and density of solar wind particles ρ_{SW}. We set $v_{\mathrm{SW}} = 400\ \mathrm{km/sec}$ and ρ_{SW} as equal to $10\ \mathrm{ions/cm^3}$ at 1au, which is assumed to be inversely proportional to the square of the distance from the Sun. Y_{SWS} is the number of particles ejected by the ion impact. Killen et al. (2001) adopted $Y_{\mathrm{SWS}} = 0.15$, but this value decreases by a factor of approximately 0.1 when considering porosity (e.g. Morgan and Killen, 1997). Y_{SWS} is routinely set as 0.06 in this study. c_{Na} is the fraction of Na atoms in the ejecta. Incident ions reach at most 10 nm depth from the surface of grains (Starukhina and Shkuratov, 2000), with the result that ions are typically prevented from penetrating the grains' interiors by the 50-100 nm thick grain rims (Noble et al., 2005). Therefore, c_{Na} is not consistent with the fraction of Na atoms in the regolith (Killen et al., 2018). The Sigmund-Thomson distribution is usually used for the energy distribution of ejected atoms by SWS:

$$f(E,\theta) = \frac{4EU}{(E+U)^3} \cos\theta \#(6)$$

The binding energy is U, being $0.27\mathrm{eV}$ in Leblanc and Johnson (2003) and this study, but $2\mathrm{eV}$ in Burger et al. (2010). The ejection rate is thought to be prominent in the cusp region. In this study, the cusp region is limited to the mid-latitude region on the dayside of both northern and southern hemispheres like **Fig. 4** following Leblanc and Johnson (2003). Though this is quite a simple assumption, it is not expected to have an impact on results since this study focuses not on the short-term variation but the seasonal variation.

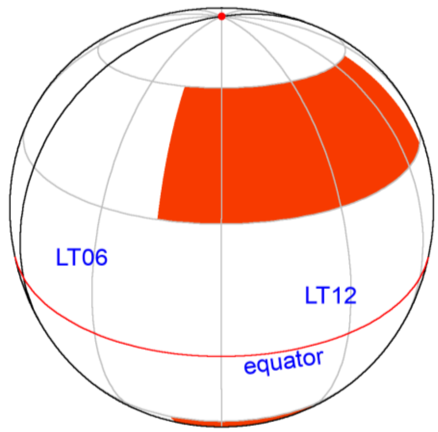

Fig. 4. SWS region in this study

3.1.4 Micrometeoroid Impact Vaporization (MIV)

When micrometeoroids strike the surface of Mercury, the impact energy causes the surface materials to evaporate, with some refractory elements. The mass of impact-induced vapor cloud for a single impact of a meteoroid with mass of M_i and velocity of V_i is given as follows (Berezhnoy and Klumov, 2008):

$$M_\mathrm{vapor}(M_\mathrm{i}, V_\mathrm{i}) = M_\mathrm{i}\left[2\left\{\frac{4}{V_\mathrm{i}}\sqrt{\frac{Q_\nu}{\nu}}\right\}^{\nu-2} - 1\right]\#(7)$$

Q_ν, the evaporation heat of the target, is taken to be $1.3\mathrm{MJ/kg}$ typical for silicates and modeling parameter ν is assumed to be 0.33 typical for continuous media. We estimate Na ejection rate by MIV using following equation:

$$R_\mathrm{MIV} = \overline{M_\mathrm{vapor}}(R)n_{mm}(R,\beta)V_0\cos Z'\, c_\mathrm{Na}/m_\mathrm{Na}\#(8)$$

$\overline{M_\mathrm{vapor}}, V_0, m_\mathrm{Na}, Z'$ are, respectively, the mean mass ejected by a single impact, the orbital speed of Mercury, the mass of a Na atom and the angle between the orbital speed vector and the position vector of a point on the surface, both of whose origins are the center of Mercury. R is the polar radial coordinate from the Sun. $\overline{M_\mathrm{vapor}}$ is turned out to be estimated by $\overline{M_\mathrm{vapor}} \fallingdotseq 7 \times 10^{-15}(R/1\mathrm{au})$ (kg/event) from numerical calculation with reference to Grotheer and Livi (2014). c_Na is equal to the fraction of Na atoms in the regolith, unlike the case of SWS. $n_{mm}(R,\beta)$ is the number density of micrometeoroids obtained from the following equation (Killen and Hahn, 2015) as a function of R and latitude β:

$$n_\mathrm{mm}(R,\beta) = \sum_j f_j R^{-\chi_j}\int_\beta^\pi \frac{h_j(i)\,\mathrm{d}i}{\sqrt{\sin^2 i - \sin^2\beta}} \times 10^{-4}(/\mathrm{m}^3)\#(9)$$

i is inclination and $h_j(i)$ represents the inclination distribution of meteoroids:

$$h_j(i) = \begin{cases} \frac{2}{\pi}\sin i \ \ c_j \exp\left(-\frac{i^2}{2\sigma_j^2}\right) & j = 1, 2 \\ \frac{2}{\pi}\sin i & j = 3 \end{cases} \#(10)$$

$j = 1$ corresponds to meteoroids from the Jupiter family comets and asteroids, $j = 2$ is from Halley type comets and $j = 3$ is from Oort cloud comets and interstellar dusts. f_j is the fraction of meteoroids derived from each source $f_1 = 0.45, f_2 = 0.50, f_3 = 0.05$. χ_j is a factor representing the dependency on the distance from the Sun: $\chi_1 = 1.00, \chi_2 = 1.45, \chi_3 = 2.00$. σ_j is the standard deviation of the distribution of meteoroids perpendicular to the dust disk: $\sigma_1 = 7°, \sigma_2 = 33°$. c_j is normalization constant: $c_1 = 10.3, c_2 = 2.19$. σ_j and c_j are not defined for $j = 3$ because Oort cloud comets and interstellar dusts can be considered to be isotopically distributed. Because the MIV ejection rate is believed to be much higher in the leading hemisphere than in the trailing hemisphere, we exclude the evening region's MIV ejection. The energy distribution of atoms ejected by MIV is usually approximated by a Maxwellian distribution of 3,000-5,000 K following the laboratory experiment of Eichhorn (1978). This study uses 3,000 K for this purpose.

3.2 Transportation processes

Three forces govern the motion of atoms in the exosphere: solar gravity, Mercury's gravity and solar radiation pressure. The equation of motion using cartesian coordinates centered on the Sun is written as follows:

$$\frac{\mathrm{d}\boldsymbol{r_0}}{\mathrm{d}t} = -\mathrm{G}\frac{M_{\mathrm{Sun}}}{r_0^3}\boldsymbol{r_0} - G\frac{M_{\mathrm{Me}}}{r_1^3}\boldsymbol{r_1} + b\frac{\boldsymbol{r_0}}{r_0} \#(11)$$

$\mathrm{G}, M_{\mathrm{Sun}}, M_{\mathrm{Me}}$ are gravitational constant, the mass of the Sun and the mass of Mercury. $\boldsymbol{r_0}$ and $\boldsymbol{r_1}$ are the position vectors of Na, as seen from the Sun and from Mercury. b is solar radiation acceleration.

3.3 Loss processes

3.3.1 Escape from Mercury's exosphere

Owing to solar radiation pressure acceleration, atoms moving at less than escape velocity can escape from Mercury's exosphere. The 6 panels in **Fig. 5** show the trajectories of test particles with various initial velocity and solar radiation pressure. Test particles are ejected from the 1 LT interval in a direction normal to the surface at a certain velocity. The initial velocity of each particle is shown in each panel. From **Fig. 5**, we can see that even atoms with an initial velocity of 3.2 km/sec, which is lower than Mercury's escape velocity (4.2 km/sec), can escape from Mercury's gravitational sphere owing to radiation acceleration and centrifugal force. Conversely, even if the velocity at the time of release is 4.4 km/sec, some particles cannot escape and re-impact the surface, especially in the dawn region.

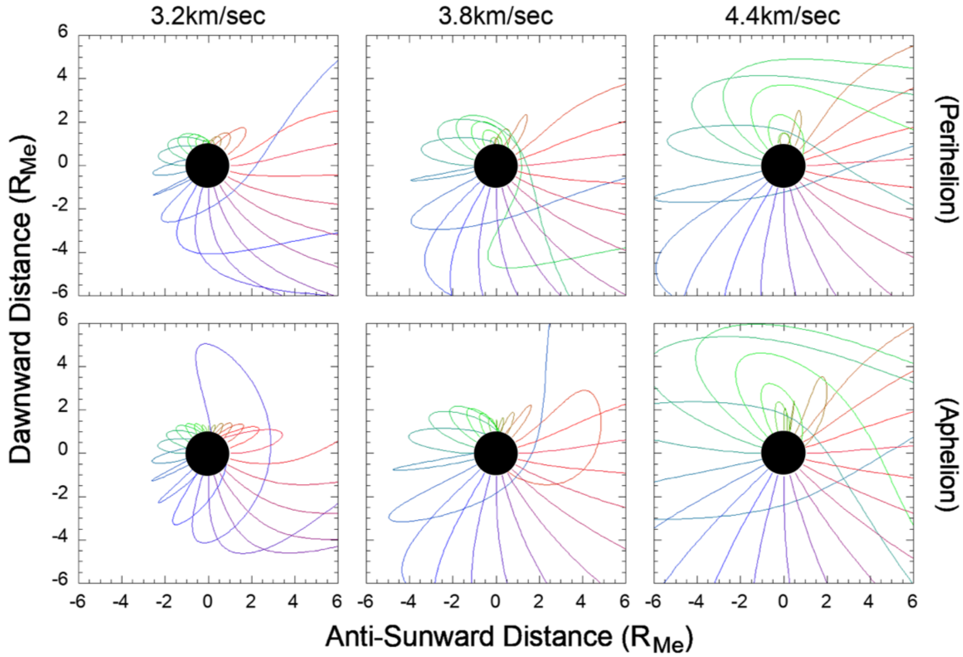

Fig. 5. Results of test particle calculation
Upper three panels are the results when Mercury is at perihelion and lower ones at aphelion. In each panel, the left is the Sun direction, the upper is dawn region and the lower is dusk region. The black circles represent Mercury. The line color differs the local time where the particle was ejected. The initial velocity of the particles are shown above each figure. The trajectories strongly depend on the TAA.

3.3.2 Re-impact on the surface

Some Na atoms that re-impact the surface are adsorbed, while TD quickly desorbs others. The adsorption rate mainly depends on surface temperature and porosity (Johnson, 2002). The adsorption rate without considering porosity is expressed as the following equation:

$$p_{\text{stick}} = A \exp\left(\frac{B}{T_s}\right) \#(12)$$

A and B are set to $A = 0.08$ and $B = 458\text{K}$ to match the Johnson (2002) experimental measurements, which shows $p_{stick} = 0.5$ at $T_s = 250$ K and $p_{stick} = 0.2$ at $T_s = 500$ K. The porosity of the rock ϕ increases the adsorption efficiency as estimated by the following equation

$$p_{\text{stick}}^{\text{eff}} = \frac{p_{\text{stick}}}{1 - (1 - p_{\text{stick}})\phi} \#(13)$$

In this study, $\phi = 0.8$ is used based on Johnson (2002). **Fig. 6** shows the temperature dependence of p_{stick} and $p_{\text{stick}}^{\text{eff}}$.

3.3.3 Photo-ionization

Neutral Na particles in the exosphere are lost by photoionization. Fulle et al. (2007) showed that photo-ionization lifetime of Na is 1.9×10^5sec at 1 au from the observation of comets. Thus, we assume that lifetime of Na until photo-ionization is calculated as $\tau =$

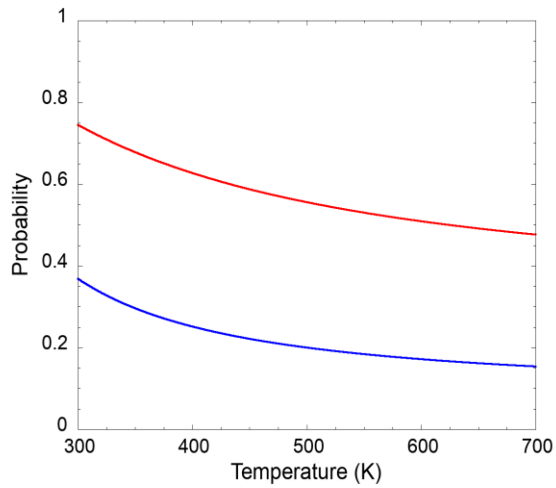

Fig. 6. Adsorption rate in re-impacting of Na atoms
The blue line corresponds the case without porosity and red line corresponds to the case considering porosity ϕ = 0.8.

$(1.9 \times 10^5 \mathrm{sec}) \times (r_0/1\mathrm{au})^2$. Coulomb collision and charge exchange are ignored since the lifetime of these reactions is several order magnitude longer than photoionization.

4 Results of numerical calculations

4.1 Altitude profile of emission

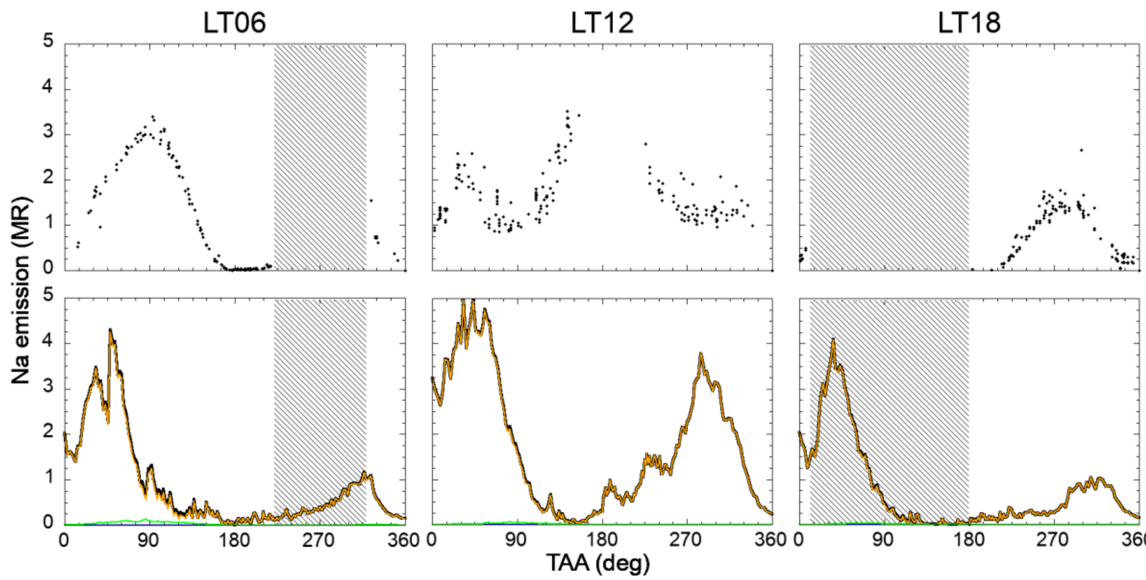

Fig. 8. Seasonal variability of Na Emission
The upper three panels are deduced from data of MASCS (same as **Fig. 2**) and the lower three panels are the results of calculation using our model. Shadow regions indicate missing data. In the lower panels, the orange line corresponds to Na derived from PSD and the black line represents the total amount of Na. The amount of Na from other processes is too small to be seen in this graph.

represents the total amount of Na. The amount of Na from TD and SWS is too small to be seen in this graph.

In this section, we compare the observations by MASCS and our model calculations in terms of the altitude profile of Na emission. For example, the altitude profiles at LT06 at TAA = 65° from both observations and model are shown in **Fig. 7**(a) and (b), respectively. The black line in **Fig. 7**(b), which is the altitude profile derived from our model, is consistent with the observations by MASCS (**Fig. 7** (a)). The rattling shape of the lines in **Fig. 7**(b) is due to the restriction on the number of particles in the model. Cassidy et al. (2015) suggests that Na below 1,000 km altitude is derived from PSD, but the main desorption process of Na above 1,000 km remains unknown. Our model shows that the dominant release process of Na is MIV (**Fig. 7** (b) green line), but SWS could also be a significant process depending on solar activity and IMF because short-term variation is observed by ground observations (Massetti et al., 2017). The number of observations of the exosphere over 1,000 km is very small. The results of the BepiColombo mission are expected.

4.2 Seasonal variability

Na radiance at an altitude of 300 km above LT06, LT12 and LT18 is shown in **Fig. 8** as a function of TAA. In terms of the seasonal variability at LT06 and LT18, the results of the calculation using the model are consistent with MASCS observations. Conversely, this model does not reproduce the emission peak at aphelion above LT12.Inconsistencies between this model and observations are considered to be due to inadequacy of the TD parameters. Most of Na at an altitude of 300 km on the dayside is derived from PSD, but as mentioned above, indirectly TD has a significant influence on Mercury's exosphere volume. Because the temperature dependence of TD varies greatly with parameters, numerical calculations with different parameters should provide different results on the seasonal variation. We performed numerical calculations again with binding energy $\mathrm{U} = 1.70, 1.85, 2.00$ eV. The results are shown in **Fig. 9**. This figure indicates that changing the TD parameters does not lower the mismatch between model and observations. Thus, it is necessary to consider a new process to understand the cause of the local and short-term increase of Na.

4.3 Additional ejection process --- the impact of Comet Dust Streams (CDS)

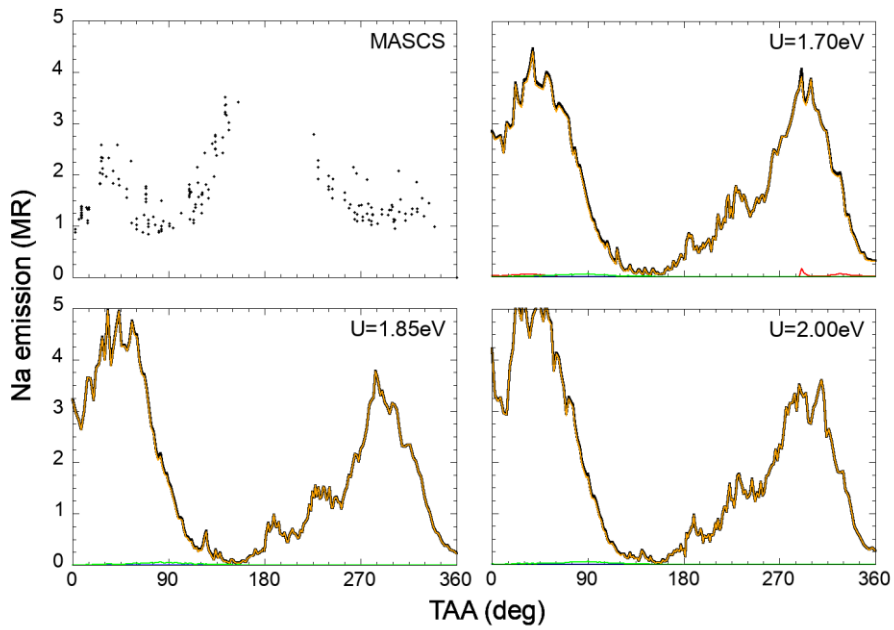

Fig. 10. The parameter dependency of the seasonal variation at LT12
The upper left panel is the observations by MASCS. The upper right is the result of model with $U = 1.70$eV, the lower left is $U = 1.85$eV and the lower right is $U = 2.00$eV.

In this study, we investigated the possibility that the ejection of Na by the impact of comet dust streams (CDS) is responsible for the maximum at the aphelion above LT12. It is found that the production rate of Ca has a peak around TAA $= 25°$ (Burger et al., 2014), and this peak is attributed to the collision of CDS derived from comet Encke (Killen and Hahn, 2015). Numerical calculation of the orbit of CDS particles of Encke shows that Ca is ejected from an area limited to less than 3% of Mercury's surface for a short period of about 10 days (Christou et al., 2015). The peak of Na at aphelion of interest in this study could be attributed to another comet-derived dust stream. Now, we calculate the seasonal variation of the amount of Na exosphere with a simple assumption of ejection by the impact of CDS. We assume that the

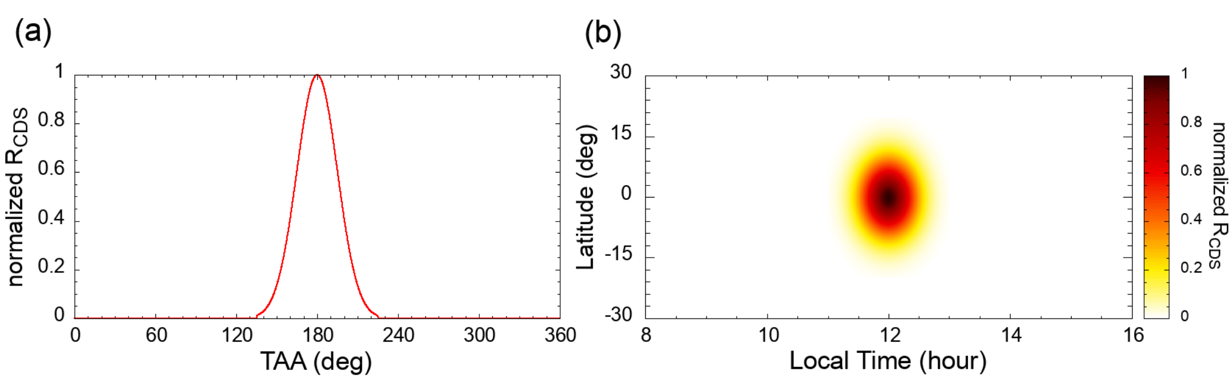

Fig. 9. (a) assumption of season of Na ejection by CDS (b) assumption of region of Na ejection by CDS
Vertical axis of (a) and color scale of (b) represent $R_{\mathrm{CDS}}/R_{\mathrm{CDS}}^{(0)}$.

ejection rate by CDS is a Gaussian distribution around TAA $= 180°$ and sub-solar point, as shown in eq.(14) and **Fig. 10**.

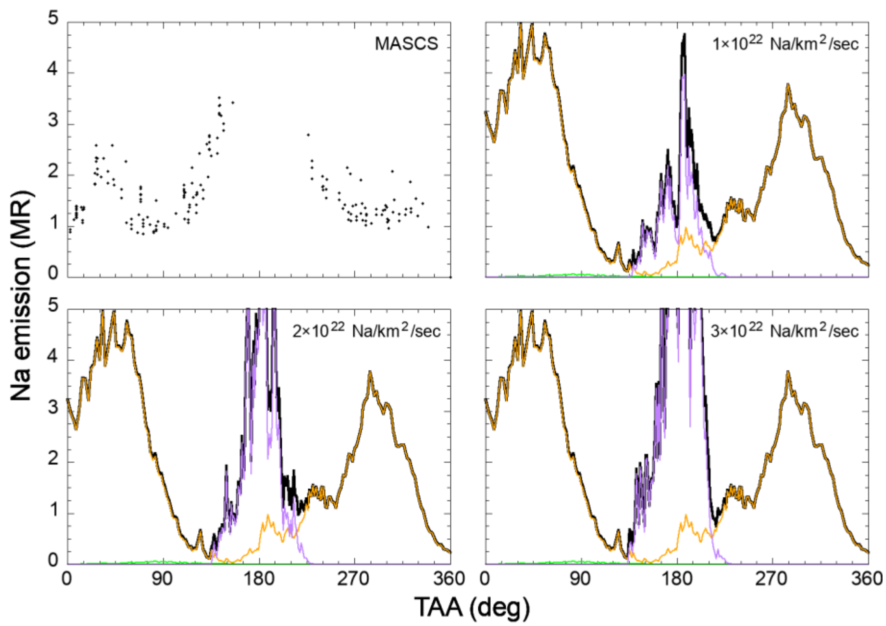

Fig. 11. Seasonal variability of Na emission at LT12 in considering CDS
The upper left panel is the observations by MASCS. The others are the results of our model. The purple line of three panels is emission of Na derived from CDS impact and the numbers at the top right of each panel are assumed values of $R_{\mathrm{CDS}}^{(0)}$.

$$R_{\mathrm{CDS}} = R_{\mathrm{CDS}}^{(0)} \exp\left\{-\frac{(\mathrm{TAA}-180°)^2}{2\sigma_{\mathrm{TAA}}^2}\right\} \exp\left[-\frac{1}{2}\left\{\frac{(\mathrm{LT}-12\mathrm{hr})^2}{\sigma_{\mathrm{LT}}^2}+\frac{\mathrm{lat}^2}{\sigma_{\mathrm{lat}}^2}\right\}\right] \#(14)$$

The initial velocity of released Na atoms is assumed to be distributed by a Maxwellian distribution of 3,000 K, as in the case of MIV. The results of the calculation with three types of $R_{\mathrm{CDS}}^{(0)}$ are shown in **Fig. 11**. This indicates that the maximum around aphelion above LT12 could be explained if there were about $R_{\mathrm{CDS}}^{(0)} \sim 10^{22}$ Na/km^2/sec, or 10^{32}Na ($\sim 5 \times 10^6$ kg) of Na ejection caused by CDS impact per Mercury year in total. From eq.(7), the released Na is about 5 wt% of the impactor in case that the velocity of the impactor is 20 km/sec, which is the mode of micrometeoroid velocity distribution. Thus, 5×10^6 kg of Na ejection corresponds to the impact of 10^8 kg of CDS in total per Mercury year. It should be noted that this is an overestimation. Since dust stream particles are expected to be faster than ordinary micrometeoroids, the mass ratio of ejected Na to impactors would be larger than 5%. Additionally CDS could contribute Na to the exosphere by increasing the supply at the surface. The amount of dust particles falling on the Earth is estimated to be about 4×10^7 kg/year (Love and Brownlee, 1993), therefore, the amount of impacting CDS predicted by our model is feasible. However, there are no observational data to support this because direct observations are lacking. Observation by MIO/MDM (Nogami et al., 2010) will provide detailed data on dust distribution around Mercury and greatly improve our understanding of the seasonal variability of Na exosphere.

5 Conclusion

Previous ground observations and simulation studies of Mercury's exosphere have shown that Na is least abundant around the aphelion and that it does not reach maximal levels at perihelion due to the depletion of surface Na by thermal desorption. Conversely, observations by MASCS onboard MESSENGER have revealed that the Na atmospheric volumes above LT12 reach their maximum near the aphelion (Cassidy et al., 2015). Three reasons have been suggested for this: (1) the rotation of the fresh ground from the nightside to the dayside, (2) the expansion of the atmosphere due to a decrease in radiation pressure, (3) the concentration of Na at the "cold-pole longitude." We also analyze the seasonal variability above LT06, LT18 to obtain results consistent with ground observations. Additionally, we attempted to reproduce the results by MASCS observations by constructing a 3D model of exosphere considering generation processes such as TD, PSD, SWS, and MIV as well as transportation and loss of Na exosphere. However, the model does not explain the peak observed around the aphelion. This indicates that a different mechanism might be necessary to account for this fact. In this study, we focus on local and short-term ejection due to the impact of comet dust streams (CDS). Numerical calculations show that the impact of less than 10^8 kg of CDS-derived dusts per Mercury year can explain the local maximum. This value is comparable to the amount of dust that falls to Earth.

This study focuses only on LT12. In the future, we will compare the calculation and observations for LTs with a small amount of observational data by using model with more realistic dust stream distribution. MDM onboard MIO included in BepiColombo mission will also provide us with important insights into the contribution of CDS to the Na exosphere. Although we only analyzed MASCS' Na observational data, comparison with Ca and Mg data by MASCS and ground observations is necessary to understand in detail the cause of the Na exosphere's seasonal variability. For example, Ca and Mg are thought to be mainly ejected by MIV (Burger et al., 2014; Merkel et al., 2017), which may greatly contribute to the generation of Na in the upper layer of the exosphere. Although the lack of observations of Na in the upper layer prevents us from a detailed understanding of MIV, observations of Ca and Mg should contribute thereto. As another example, the short-term variation noted by ground observation, which is thought to be derived from the variation of IMF (Massetti et al., 2017), can never be detected by MASCS because of the length of the observation interval. It is essential to compare variously obtained data and to evaluate them from diverse perspectives. MSASI (Yoshikawa et al., 2010) onboard MIO will observe Na exosphere through the detection of D2 line of Na in BepiColombo mission. The data will also provide us critical insight about the seasonal variability of Na exosphere.

Acknowledgments, Samples, and Data

Original data reported in this paper are archived by the NASA Planetary Data System (https://pds-geosciences.wustl.edu/missions/messenger/mascs.htm).

References

Berezhnoy, A. A., & Klumov, B. A. (2008), Impacts as sources of the exosphere on Mercury. *Icarus*, 195, 511-522. doi:10.1016/j.icarus.2008.01.005

Burger, M. H., et al. (2010), Monte Carlo modeling of sodium in Mercury's exosphere during the first two MESSENGER flybys. *Icarus*, 209, 63-74. doi:10.1016/j.icarus.2010.05.007

Burger, M. H., Killen, R. M., McClintock, W. E., Merkel, A. W., Vervack Jr., R. J., Cassidy, T. A., & Sarantos, M. (2014), Seasonal variations in Mercury's dayside calcium exosphere. *Icarus*, 238, 51-58. doi:10.1016/j.icarus.2014.04.049

Cassidy, T. A., & Johnson, R. E. (2005), Monte Carlo model of sputtering and other ejection processes within a regolith. *Icarus*, 176, 499-507. doi:10.1016/j.icarus.2005.02.013

Cassidy, T. A., Merkel, A. W., Burger, M. H., Sarantos, M., Killen, R. M., McClintock, W. E., & Vervack Jr., R. J. (2015), Mercury's seasonal sodium exosphere: MESSENGER orbital observations. *Icarus*, 248, 547-559. doi:10.1016/j.icarus.2014.10.037

Cassidy, T. A., McClintock, W. E., Killen, R. M., Sarantos, M., Merkel, A. W., Vervack Jr., R. J., & Burger, M. H. (2016), A cold-pole enhancement in Mercury's sodium exosphere. *Geophys. Res. Lett.*, 43, 11,121-11,128. doi:10.1002/2016GL071071

Chamberlain, J. W. (1963), Planetary coronae and atmospheric evaporation. *Planet. Space Sci.*, 11, 911-960. doi:10.1016/0032-0633(63)90122-3

Chase, S. C., Miner, E. D., Morrison, D., Münch, G., & Neugebauer, G. (1976), Mariner 10 Infrared Radiometer results: temperatures and thermal properties of the surface of Mercury. *Icarus*, 28, 655-678. doi:10.1016/0019-1035(76)90130-5

Christou, A. A., Killen, R. M., & Burger, M. H. (2015), The meteoroid stream of comet Encke at Mercury: implications for MErcury Surface, Space ENvironment, GEochemistry, and Ranging observations of the exosphere. *Geophys. Res. Lett.*, 42, 7311-7318. doi:10.1002/2015GL065361

Delcourt, D. C., et al. (2003), A quantitative model of the planetary Na+ contribution to Mercury's magnetosphere. *Ann. Geophys.*, 21, 1723-1736. doi:10.5194/angeo-21-1723-2003

Eichhorn, G. (1978), Heating and vaporization during hypervelocity particle impact. *Planet. Space Sci.*, 26, 463-467. doi:10.1016/0032-0633(78)90067-3

Fulle, M., et al. (2007), Discovery of the atomic iron tail of comet McNaught using the heliospheric imager on *STEREO*. *Astrophys. J.*, 661, L94-96.

Grotheer, E. B., & Livi, S. A. (2014), Small meteoroids' major contribution to Mercury's exosphere. *Icarus*, 227, 1-7. doi:10.1016/j.icarus.2013.07.032

Hunten, D. M., & Sprague, A. L. (1997), Origin and character of the lunar an Mercurian atmospheres. *Adv. Space Res.*, 19, 1551-1560. doi:10.1016/S0273-1177(97)00368-2

Hunten, D. M., & Sprague, A. L. (2002), Diurnal variation of sodium and potassium at Mercury. *Meteorit. Planet. Sci.*, 37, 1191-1195. doi:10.1111/j.1945-5100.2002.tb00888.x

Johnson, R. E. (2002), Surface boundary layer atmospheres. In: Mendillo, M., Nagy, A., Waite, J.H. (Eds.), *Atmosphere in the Solar System: Comparative Aeronomy*, 203-219, Washington, DC, American Geophysical Union.

Killen, R. M., Potter, A. E., Reiff, P., Sarantos, M., Jackson, B. V., Hick, P., & Giles, B. (2001), Evidence for space weather at Mercury. *J. Geophys. Res.*, 106, 20,509-20,525. doi:10.1029/2000JE001401

Killen, R.M., Sarantos, M., Potter, A. E., & Reiff, P. (2004), Source rates and ion recycling rates for Na and K in Mercury's atmosphere. *Icarus*, 171, 1-19. doi:10.1016/j.icarus.2004.04.007

Killen, R. M., & Hahn, J.M. (2015), Impact vaporization as a possible source of Mercury's calcium exosphere. *Icarus*, 250, 230-237. doi:10.1016/j.icarus.2014.11.035

Killen, R. M., Burger, M. H., Vervack Jr., R. J., & Cassidy, T. A. (2018), Understanding Mercury's exosphere: models derived from MESSENGER observations. 15; Chapter. In: Solomon S.C., Nittler, L.R., Anderson, B.J., (Eds.), *Mercury: The View after MESSENGER*, 407-429, Cambridge Univ. Press.

Leblanc, F., & Johnson, R. E. (2003), Mercury's sodium exosphere. *Icarus*, 164, 261-281. doi:10.1029/2003JE002151

Leblanc, F., & Johnson, R. E. (2010), Mercury exosphere I. Global circulation model of its sodium component. *Icarus*, 209, 280-300. doi:10.1016/j.icarus.2010.04.020

Love, S. G., & Brownlee, D. E. (1993), A direct measurement of the terrestrial mass accretion rate of cosmic dust. *Science*, 262, 550-553. doi: 10.1126/science.262.5133.550

Massetti, S., Mangano, V., Millio, A., Mura, A., Orsini, S., & Plainaki, C. (2017), Short-term observations of double-peaked Na emission from Mercury's exosphere. *Geophys. Res. Lett.*, 44, 2970-2977. doi:10.1002/2017GL073090

McClintock, W.E., & Lankton, M.R. (2007), The Mercury Atmospheric and Surface Composition Spectrometer for the MESSENGER mission. *Space Sci. Rev.*, 131, 481-521. doi:10.1007/s11214-007-9264-5

Merkel, A. W., Cassidy, T. A., Vervack Jr., R. J., McClintock, W. E., Sarantos, M., Burger, M. H., & Killen, R. M. (2017), Seasonal variations of Mercury's magnesium dayside exosphere from MESSENGER observations. *Icarus*, 281, 46-54. doi:10.1016/j.icarus.2016.08.032

Morgan, T. H., & Killen, R. M. (1997), A non-stoichiometric model of the composition of the atmospheres of Mercury and the Moon. *Planet. Space Sci.*, 45, 81-94. doi:10.1016/S0032- 0633(96)00099-2

Mura, A., et al. (2009), The sodium exosphere of Mercury: comparison between observations during Mercury's transit and model results. *Icarus*, 200, 1-11. doi:10.1016/j.icarus.2008.11.014

Noble, S.K., Keller, L. P., & Pieters, C. M. (2005), Evidence of space weathering in regolith breccias I: lunar regolith breccias. *Meteorit. Planet. Sci.*, 40, 397-408. doi:10.1111/j.1945-5100.2005.tb00390.x

Nogami, K., et al. (2010), Development of the Mercury dust monitor (MDM) onboard the BepiColombo mission. *Planet. Space Sci.*, 58, 108-115. doi:10.1016/j.pss.2008.08.016

Schleicher, H., Wiedemann, G., Wöhl, H., Berkefeld, T., & Soltau, D. (2004), Detection of neutral sodium above Mercury during the transit on 2003 May 7. *Astron. Astrophys.*, 425, 1119-1124. doi:10.1051/0004-6361:200 40477

Starukhina, L.V., & Shkuratov, Y.G. (2000), The luner poles: water ice or chemically trapped hydrogen? *Icarus*, 145, 585-587. doi:10.1006/ icar.2000.6476.

Vilas, F. (1988), Surface composition of Mercury from reflectance spectrophotometry. *Mercury*, 59-76.

Wang, W.C., & Ip, W.H. (2011), Source dependency of exospheric sodium on Mercury. *Icarus*, 216, 387-402. doi:10.1016/j.icarus.2011.09.023

Wiens, R. C., Burnett, D. S., Calaway, W. F., Hansen, C. S., Lykke, K. R., & Pellin, M. J. (1997), Sputtering products of sodium sulfate: implications for Io's surface and for sodium-bearing molecules in the Io torus. *Icarus*, 128, 386-397. doi:10.1006/icar.1997.5758

Yakshinskiy, B.V., & Madey, T.E. (1999), Photon-stimulated desorption as a substantial source of sodium in the lunar atmosphere. *Nature*, 400, 642– 644. doi:10.1038/23204

Yakshinskiy, B.V., & Madey, T.E. (2004), Photon-stimulated desorption of Na from a lunar sample: Temperature dependent effects. *Icarus*, 168, 53–59. doi:10.1016/j.icarus.2003.12.007

Yoshikawa, I., et al.（2010), The Mercury sodium atmospheric spectral imager for the MMO spacecraft of Bepi-Colombo. *Planet. Space Sci.*, 58, 224-237. doi:10.1016/j.pss.2008.07.008